Water Resources and Industry 20 (2018) 1–14

Contents lists available at ScienceDirect

Water Resources and Industry

journal homepage: www.elsevier.com/locate/wri

Reclamation of water and the synthesis of gypsum and limestone from acid mine drainage treatment process using a combination of pre-treated magnesite nanosheets, lime, and CO_2 bubbling

Vhahangwele Masindi[a,b,*], Godfrey Madzivire[b,c], Memory Tekere[b]

[a] Council for Scientific and Industrial Research (CSIR), Built Environment (BE), Hydraulic Infrastructure Engineering (HIE), P.O Box 395, Pretoria 0001, South Africa

[b] Department of Environmental Sciences, School of Agriculture and Environmental Sciences, University of South Africa (UNISA), P. O. Box 392, Florida 1710, South Africa

[c] Council for Geoscience, Water and Environment Unit, 280 Pretoria Street, Silverton, Pretoria, South Africa

ARTICLE INFO

Keywords:
Acid mine drainage
Magnesite
Gypsum
Limestone
Carbon dioxide

ABSTRACT

In this study, an integration of pre-treated magnesite, lime, and CO_2 bubbling (MLC) was used for the treatment of acid mine drainage (AMD). The primary aim was to reclaim clean water and synthesize valuable minerals. This treatment process comprises three steps which include neutralisation (i) using magnesite, gypsum synthesis (ii) using lime and limestone synthesis (iii) using CO_2 bubbling. Reactors at a semi-pilot scale system were used to fulfil the goals of this study. AMD was mixed with magnesite and lime at 1 g: 100 mL S/L and 8 g: 100 mL S/L ratios respectively. Pilot results revealed that amorphous hydroxides of Fe, gypsum, and limestone can be obtained from the secondary sludge/product. The obtained materials were of high purity (> 75%). This was further confirmed by X-ray Diffraction, X-ray Fluorescence, and Fourier Transform Infrared Spectrometer analytical techniques. The product water was suitable for irrigation, industrial and agricultural use as per South African standards. Furthermore, it was observed that the initial pH of AMD was 2.5 and it was increased to pH ≥ 10 and > 12 after contacting magnesite and lime respectively. To stabilise the pH, CO_2 was bubbled and the pH was reduced to ≤ 7.29 which was suitable for a number of applications. Moreover, ≥ 99% and ≥ 95% of metal species and sulphate were removed from an aqueous system, respectively. The techno-economic evaluation indicated that it can cost R806.40 (66 USD) to treat 3.5 KL of acid mine drainage and have a return of R11263.60 (933 USD) from the selling of the recovered materials, thus making this technology economically viable. From the findings of this study, it can be concluded that the application of MLC process can neutralise AMD and produce valuable products. More so, this novel and self-sustainable project will therefore go a long way in curtailing the impacts of AMD by valorising the product minerals and exploit the resultant commercial value hence aiding in off-setting the running costs of the treatment process.

* Corresponding author at: Council for Scientific and Industrial Research (CSIR), Built Environment (BE), Hydraulic Infrastructure Engineering (HIE), P.O Box 395, Pretoria 0001, South Africa.

E-mail addresses: VMasindi@csir.co.za, masindivhahangwele@gmail.com (V. Masindi).

https://doi.org/10.1016/j.wri.2018.07.001
Received 22 November 2017; Received in revised form 7 May 2018; Accepted 11 July 2018

1. Introduction

Depending on hydrogeology, mine effluents have different physicochemical properties that range from acidic, neutral and basic drainage [1–3]. Amongst those, acid mine drainage (AMD) forms the crux of the largest liabilities faced by the mining industry due to the extent of potential impacts, scale and magnitudes of its threat to water resources, human health and the environment [4–7]. Acid mine drainage results from the weathering of pyrite (FeS_2) and other reactive sulphide-bearing minerals when exposed to atmospheric air and water leading to the release of a drainage that is rich in acid, sulphate and metal ions into the environment [8,9], as shown in Fig. 1(A) and (B). These minerals may be embedded in the tailings or host rocks of a mineral in quest. As such, AMD can be formed from the tailings seepage (Fig. 1(**B**)) or decanting from underground voids (Fig. 1**(A)**).

Acid mine drainage is primarily composed of H^+, SO_4^{2-}, and Fe(II), as the major components [10]. Masindi, Gitari, Tutu and DeBeer [11] further pointed out that AMD also contains Al(III) and Mn(II), As, Cu, Ni, Zn, Co and Cr and alkaline earth metals such as Mg and Ca. The formation of AMD may be depicted by the following chemical equation [12,13]:

$$4FeS_2 + 15O_2 + 14H_2O \xrightarrow{\text{bacteria}} 4Fe(OH)_3 + 8SO_4^{2-} + 16H^+ \quad (1)$$

High acidity in secondary water increases the solubility, mobility and bio-availability of metals species, hence raising the concentration to unacceptable, and often, toxic levels [4,8,14]. The adverse effects of acidification on aquatic ecosystems are associated with deteriorating quality of water in the receiving environment, destruction of the bicarbonate buffer (neutralizing) capacity of water, the loss of bicarbonate-dependant photosynthetic organisms as bicarbonate is consumed, the reduction and eventual cessation of nutrient cycling processes in water bodies, and loss of organisms through damage to carbonate exoskeletons or cell components [15,16]. The most visual legacy of AMD is undoubtedly the precipitation of ferric (Fe^{3+}) hydroxide and oxy-hydroxide and oxy-hydrosulphates complexes as a yellow or orange coating in stream channels [17,18]. These precipitates lead to a reduction in dissolved oxygen concentrations in affected water bodies during their formation, and have abrasive effects on biota and clog streambeds once formed. It can also prevent the penetration of light to aquatic ecosystem, hence suffocating aquatic organisms [19–23].

In South Africa, recent studies have reported that there are enormous volumes of AMD produced by the Western Basin on the West Rand basin in Gauteng Province that amount to ~60 mL/d, carrying sulphate (SO_4) concentrations of ~4.5–5 g/L and ferrous iron (Fe^{2+}) concentrations of up to ~1.5 g/L depending on seasons and host rock, during and after rainfall it can even go beyond that limit [2,10]. The Mpumalanga coal basins can have up to ± 18 g/L of sulphate and ± 6 g/L of Fe-species [10,18,24].

Worldwide, a number of treatment methods, both passive and active, have been proposed and used for abating AMD [4,14,25–29]. Among these, the common ones include ion-exchange [30–32], adsorption [33–38], bio-sorption [39–43], bio-precipitation [44–47], neutralisation [29,48–53], coagulation and precipitation [54–59]. The extent of application of most of these methods has largely been limited by factors such as cost and generation of excessive secondary sludge [14,16,31,60–64]. Adsorption has been regarded as the best technology for water depollution but its effectiveness is limited to dilute solutions due to quick saturation of the adsorbent and selective adsorption. In light of the above, precipitation of chemical species coupled with adsorption has received paramount attention lately. This is attributed to its ability to treat large volumes of water with high efficiency.

The principal aim of this study was to treat AMD using calcined cryptocrystalline magnesite. The treated water was taken to subsequent reactors for gypsum and limestone synthesis. The resale of recovered products will off-set the running cost of this technology, hence making it to be self-sustainable. This integrated approach has three phases of water treatment and they include: (i) neutralisation and metals removal using calcined cryptocrystalline magnesite, (ii) gypsum synthesis in the secondary process using lime and (iii) bubbling of CO_2 into the third reactor to synthesize limestone. The product water is anticipated to meet the discharge and irrigation requirements as per regulatory frameworks.

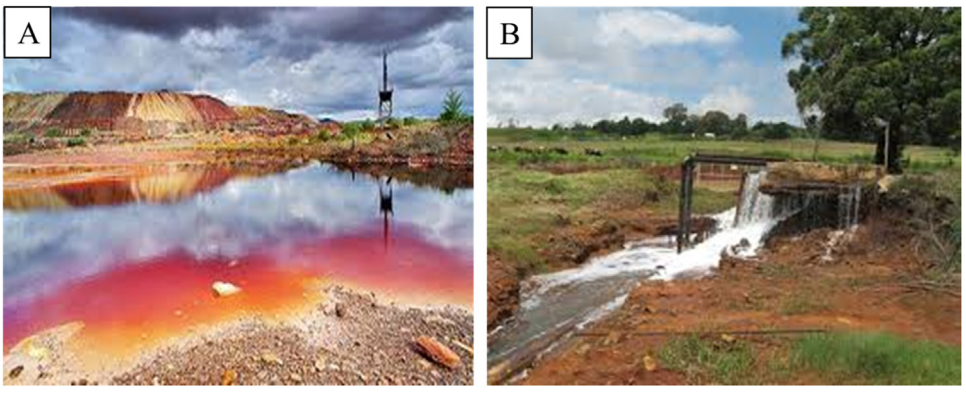

Fig. 1. AMD from tailings leachates (A) and underground shaft decant (B).

2. Materials and methods

2.1. Sampling and reagents acquisition

Raw AMD generated from coal washing and mining processes in Mpumalanga Province, South Africa, was collected and sealed in high-density polyethylene (HDPE) plastic bottles until utilisation for the defined purpose. The solids and debris in the water samples were removed by filtration. Industrial grade lime and calcined cryptocrystalline magnesite were obtained from Protea Chemical Pty (Ltd), South Africa. Carbon dioxide (CO_2) was obtained from AFROX gas supplying company in South Africa, Pty (Ltd).

2.2. Characterisation of feed and product materials

The pH, Total Dissolved Solids (TDS) and Electrical Conductivity (EC) were monitored using CRISON MM40 portable pH/EC/TDS/Temperature multimeter probe. Multi-elemental analysis was performed by ICP-MS (7500ce, Agilent, Alpharetta, GA, USA). The accuracy of the analysis was monitored by analysis of National Institute of Standards and Technology (NIST) water standards. Mineralogy of synthesized materials were determined using X-ray Diffraction (XRD) (Philips PW 1710 Diffractometer; graphite secondary monochromatic source). Elemental constituents were evaluated using X-ray fluorescence (XRF) (Thermo Fisher ARL-9400 XP + Sequential XRF equipped with WinXRF software). Morphological properties were determined using an Auriga Cobra FIB FESEM instrument high resolution scanning electron microscope (HR- SEM) with the precision milling and nanofabrication abilities of high resolution focused ion beam (FIB) at an accelerating voltage of 3 KeV (Model: Sigma VP FE-SEM with Oxford EDS Sputtering System, Make: Carl Zeiss, Supplier: Carl Zeiss, USA). Mapping of gypsum was ascertained using High Resolution Transmission Electron Microscopy (HR-TEM) (JEM – 2100 electron microscope, Angus Crescent, The Netherlands). Functional groups and their wave-numbers were identified by Perkin-Elmer Spectrum 100 Fourier Transform Infrared Spectrometer (FTIR) equipped with a Perkin-Elmer Precisely Universal Attenuated Total Reflectance (ATR) sampling accessory equipped with a diamond crystal. The thermal stability of the materials was determined using a Thermo Gravimetric Analyser (TGA Q500, TA instrument) under air atmosphere with a flow rate of 50 mL/min and a heating rate of 10 °C/min. Surface area analysis was done using Brunauer-Emmet-Teller (BET) with micromeritics VacPrep 061 equipped with a −195.800 °C liquid nitrogen bath and samples degassing system (Micromeritics Tri-Star II, Surface area and porosity, Poretech cc, USA). Degassing of samples was done at 100 °C for 20 h.

2.3. Treatment of field AMD at optimized conditions

An integrated process for the treatment of acid mine drainage is depicted by Fig. 2 below.

As shown in Fig. 2, calcined cryptocrystalline magnesite, lime and CO_2 bubbling (MLC process) was used to recover valuable minerals that have commercial value and to produce water that is fit for many defined uses such as irrigation and industrial processes. The minerals recovery and water reclamation process used authentic AMD from coal mining processes. A sequential and fractional precipitation approach was employed to precipitate metals as hydroxide in the first reactor.

Masindi, Gitari, Tutu and De Beer [9] reported that the interaction of magnesite with AMD lead to the precipitation of metals as hydroxides (solids). Magnesium formed a complex of $MgSO_{4\ (1)}$ on contact with sulphate rich mine water (Eq. (3)). The sulphate was taken to a lime reactor. Interaction of lime and magnesium sulphate will lead to the formation of gypsum (solids) as shown by the reactions below [65,66]:

$$CaO + H_2O \rightarrow Ca(OH)_2 \quad (2)$$

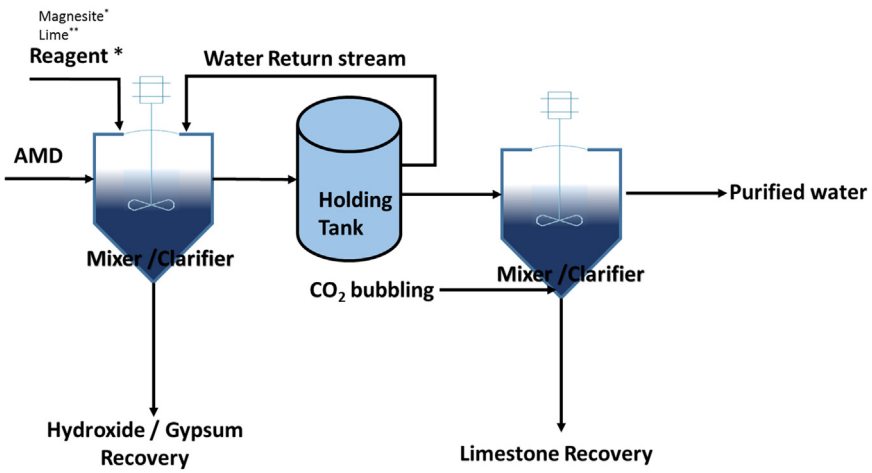

Fig. 2. Treatment process for the treatment of AMD using MLC process. **Note:** *) = Step 1: AMD neutralisation by calcined cryptocrystalline magnesite. **) = Step 2: Gypsum synthesis by lime.

$$MgSO_{4(l)} + Ca(OH)_{2(s)} + H_2O \rightarrow Mg(OH)_{2(s)} + CaSO_4.H_2O_{(s)} \quad (3)$$

For formation of gypsum, Eq. (3), as a result of ion exchange between $MgSO_{4(l)}$ and $Ca(OH)_{2(s)}$, the following applies:

Species present:	Mg^{2+} ions and SO_4^{2-} ions	(from $MgSO_4$ complex)
	Ca^{2+} ions and OH^- ions	(from $Ca(OH)_2$)
	H^+ ions and OH^- ions	(from dissociation of water)
	H_2O molecules	(solvent)
Species that could be reduced:	Mg^{2+} ions	
	Ca^{2+} ions	
	H^+ ions (Negligible, because concentration is low as the mixture is very alkaline at this stage)	
	H_2O molecules	

As H_2O molecules have the highest standard potential compared to Mg^{2+} ions and Ca^{2+} ions, they will be reduced.

$$\text{Reduction} - \text{half reaction: } 2H_2O_{(l)} + 2e^- \rightarrow H_{2(g)} + 2OH^-_{(aq)} \quad (4)$$

Mg^{2+} has a higher standard potential than Ca^{2+} ions, and OH^- ions have the lowest standard potential SO_4^{2-} ions. Therefore, Mg^{2+} will bond with OH^- ions and Ca^{2+} with SO_4^{2}.

Species that could be oxidised:	SO_4^{2-} ions
	OH^- ions (Negligible)
	H_2O molecules

As OH^- ions have the lowest standard potential than the other species, but their concentration is negligible due to high concentration of SO_4^{2-} ions in the medium.

$$\text{Oxidation} - \text{half reaction: } 2H_2O_{(l)} \rightarrow O_{2(g)} + 4H^+ + 4e^- \quad (5)$$

To balance the two half reactions, the oxidation-half reaction is multiplied by 2.

$$\text{Overall (redox) reaction: } 6H_2O_{(l)} \rightarrow O_{2(g)} + 4H^+ + 2OH^- + 2H_{2(g)} \quad (6)$$

This makes sense as the introduction of H^+ reduces the pH of the medium as the reaction proceeds further with continuous precipitation of magnesium and calcium, which contribute to high alkalinity. The produced H^+ and OH^- ions form water that has undergone treatment. The pH is further reduced by CO_2 (Eq. (7))

The residual calcium reacted with CO_2 to stabilise the pH and remove Ca as limestone as shown in Eq. (4).

$$CO_{2(g)} + Ca^{2+}_{(aq)} + H_2O \rightarrow CaCO_{3(s)} + 2H^+ \quad (7)$$

In this reaction chemistry and thermodynamics, $CO_{2\ (g)}$ is a typical acid forming gas because when it dissolves in water, it forms carbonic acid. The cationic acid donates the protons (hydrogen ions) and form bicarbonate ions. The bicarbonate ions donates protons and generates a carbonate ion

$$CO_2 + H_2O \leftrightarrow H_2CO_{3(aq)} \quad (8)$$

$$H_2CO_{3(aq)} \leftrightarrow HCO^-_{3(aq)} + H^+_{(aq)} \quad (9)$$

$$HCO^-_{3(aq)} \leftrightarrow CO^{2-}_{3(aq)} + H^+_{(aq)} \quad (10)$$

The equilibrium constant at room temperature for Eqs. (5) and (6) could be written as:

$$K_1 = \frac{[HCO_3^-][H^+]}{H_2CO_3} = 10^{-6.37}, K_2 = \frac{[CO_3^{2-}][H^+]}{HCO_3^-} = 10^{-10.26} \quad (11)$$

That is the reason the pH of the water was reduced to ≤ 7.3 which is suitable for other defined uses.

2.3.1. Neutralization of AMD

Field AMD samples were treated using calcined cryptocrystalline magnesite at 60 mins of equilibration, 1 g: 100 mL S/L ratios, 650 rpm shaking speed and ≤ 32 μm particle size as reported by Masindi, Gitari, Tutu and De Beer [12]. Physico-chemical parameters were determined as mentioned in Section 2.2. Validity of the obtained results was maintained by inter-laboratory analysis (in accredited laboratories) and executing experiments in triplicate with the data reported as mean value.

2.3.2. Synthesis of gypsum

An industrial grade lime was used as a precursor for synthesis of gypsum. Lime was added to magnesite-treated water which is

Table 1
Chemical compositions of AMD before and after contacting magnesite, lime reacted water and CO_2 bubble water.

Element	Units	Raw	Magnesite	Lime	CO bubbling	% Removal	WHO	DWS
Aluminium	mg/L Al	60	0.1	< 0.1	0.1	99.83	0.1	5
Ammonia	mg/l NH_3	8	5	2	1	87.50	0.2	2
Antimony	mg/L Sb	0.1	0.1	< 0.1	0.1	0.00	0.02	0.1
Arsenic	mg/L As	0.1	< 0.1	< 0.1	0.1	0.00	0.01	0.1
Barium	mg/L Ba	0.1	0.1	< 0.1	0.1	0.00	0.7	N/A
Boron	mg/l B	0.02	0.21	0.11	0.01	50.00	0.5	0.5
Cadmium	mg/L Cd	0.1	0.1	< 0.1	0.1	0.00	0.003	10
Chloride	mg/l Cl	4.1	2	6.6	1.2	70.73	0.7	1
Chlorine (free)	mg/l Cl_2	0.07	< 0.020	< 0.02	0.03	57.14	5	N/A
Chromium	mg/L Cr	1	0.1	< 0.1	0.1	90.00	0.05	0.1
Colour	mg/l Pt	363	8	9	24	93.39	N/A	N/A
Copper	mg/L Cu	0.5	0.1	< 0.1	0.1	80.00	2	0.2
Cyanide total	mg/l CN	0.02	< 0.010	< 0.01	0.01	50.00	0.07	N/A
Conductivity	mS/m	1018	1128	913	27.7	97.28	N/A	N/A
Fluoride	mg/l F	0.2	< 0.20	< 0.20	0.2	0.00	1.5	2
Iron	mg/L Fe	2000	< 0.1	0.1	0.1	100.00	2	5
Lead	mg/L Pb	0.1	< 0.1	0.1	0.1	0.00	0.01	0.2
Manganese	mg/L Mn	100	< 0.1	0.1	0.01	99.90	0.4	0.02
Mercury	mg/L Hg	1	< 0.1	0.1	0.01	99.00	0.006	N/A
Monochloramine	mg/l Cl_2	0.04	0.41	0.01	0.01	75.00	0.7	N/A
Nickel	mg/L Ni	5	< 0.1	0.1	0.1	98.00	0.07	0.2
Nitrate + Nitrite	mg/l N	0.2	< 0.20	0.20	0.2	0.00	50	10
Nitrate Nitrogen	mg/l N	0.2	< 0.20	0.20	0.2	0.00	50	0.5
Nitrite Nitrogen	mg/l N	0.2	< 0.20	0.20	0.2	0.00	50	0.5
pH	pH	2.55	10	12	7.3	N/A	6.5–9.5	6.4–8.4
Selenium	mg/L Se	0.1	< 0.1	< 0.1	0.1	0.00	0.01	0.02
Sodium	mg/l Na	0.1	< 0.1	< 0.1	0.1	0.00	20	70
Sulphate	mg/l SO_4	11,789	9079	79	50	99.58	500	N/A
TDS	mg/l	15,000	5990	3840	735	95.10	N/A	N/A
Turbidity	NTU	789	< 10	< 10	10	98.73	N/A	N/A
Uranium	mg/L U	765	< 0.1	< 1.0	1	99.87	0.015	0.01
Zinc as Zn	mg/L Zn	14	< 0.1	< 1.0	1	92.86	0.05	1

Note: DWS stand for the Department of Water and Sanitation and WHO stand for World Health Organisation.

rich in magnesium sulphate. Specified grams of lime were added into the reactor at 8 g: 100 mL S/L ratios as reported by Benatti, Tavares and Lenzi [67]. The mixture was equilibrated at 650 rpm shaking speed for 60 mins using an overhead stirrer. The resultant residues and water were taken for analysis as described in Section 2.2.

2.3.3. Synthesis of limestone

An industrial grade Carbon dioxide (CO_2) from Afrox was used for precipitation of limestone ($CaCO_3$). Carbon dioxide was bubbled through magnesite treated water from the bottom of the reactor as shown in Fig. 2. The pH meter was also dipped into water to monitor the pH fluctuations. Due to legislative requirements, the targeted pH was maintained at a range of ≈ 7–7.5. The resultant residues and water were taken for analysis as described in Section 2.2.

3. Results and discussion

3.1. Treatment of authentic AMD effluents

The chemical compositions of AMD before and after contacting magnesite, lime reacted water and CO_2 bubble water are shown in Table 1.

The initial pH of AMD used in this study was observed to be 2.5. It was therefore increased to 10, 12, and 7.3 after using calcined cryptocrystalline magnesite, lime and CO_2 bubbling, respectively. The Total dissolved solids (TDS) and electrical conductivity (EC) were also observed to have decreased on a stepwise fashion for magnesite, lime and CO_2 treated waters. A reduction in TDS and EC may be attributed to precipitation of notable quantities of dissolved metal species and sulphates from aqueous system. The sulphate recorded in this sample was 11,789 mg/L making this anion dominant. Major cations included Ca, Mg, Al, Mn and Fe. The predominance of Fe and SO_4^{2-} indicated that this mine water was subjected to pyrite oxidation. From the obtained results, the treated water is suitable for irrigation as shown in the DWS water quality guidelines. Some parameters were within the WHO waste quality standard hence requiring the water to be further treated for it to meet the drinking water quality specifications.

3.2. Mineralogy characterisation

The mineralogical compositions of hydroxides, gypsum and limestone are presented in Fig. 3.

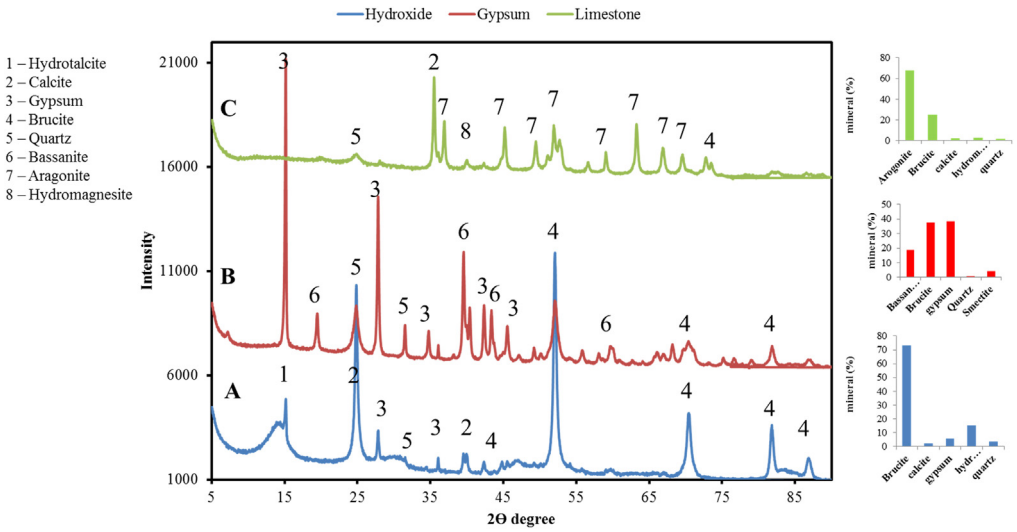

Fig. 3. XRD spectra of hydroxides, gypsum and limestone.

As shown in Fig. 3**(A)**, the product from the magnesite reactor was rich in brucite, gypsum, calcite, quartz and hydrotalcite. This may be attributed to the formation of gypsum from the reaction of Ca and sulphate in water. Brucite may be originating from the precipitation of magnesium from solution. Quartz is from feed magnesite as reported in literature [68]. The reaction of magnesite treated water resulted in the formation of basanite, gypsum, brucite, quartz and montmorillonite (Fig. 3**(B)**). Calcium sulphate constituted 57.24% and brucite was 37.66%. This may be explained by the information in literature, that indicates that Mg precipitates at pH > 10 [69]. The rest were impurities of Si and Al. As shown in Fig. 3**(C)**, the synthesis of limestone yielded a high purity material. Similar results were reported by Benatti, Tavares and Lenzi [67]. As shown in Fig. 3**(C)**, aragonite and brucite were the major components. This may be attributed to the reaction of carbon dioxide with calcium leading to the formation of calcium carbonate. Moreover, hydromagnesite was also observed hence indicating that carbon dioxide is also reacting with residual magnesium. The purity of limestone is 70.45% and fractions of magnesium based materials (27.94%) hence making this product the best candidate for agricultural purposes.

3.3. X-ray fluorescence analysis

The elemental composition (wt%) of hydroxides, gypsum and limestone are shown in Table 2.

As shown in Table 2, the elemental composition (wt%) of synthesized hydroxides, gypsum and limestone. After the interaction of

Table 2
Elemental composition (wt%) of hydroxides, gypsum and limestone against certified materials.

Element (wt%)	Certified	Analysed	Hydroxides	Gypsum	Limestone
SiO_2	**99.6**	99.70	11.90	0.02	1.64
TiO_2	**0.01**	0.00	0.42	< 0.01	0.05
Al_2O_3	**0.05**	0.01	7.52	< 0.01	0.87
Fe_2O_3	**0.05**	0.01	20.10	0.05	2.51
MnO	**0.01**	0.00	3.61	< 0.01	0.34
MgO	**0.05**	0.01	7.47	10	1.10
CaO	**0.01**	0.01	36.90	58.00	67.40
Na_2O	**0.05**	0.02	< 0.01	0.20	< 0.01
K_2O	**0.01**	0.01	< 0.01	< 0.01	< 0.01
P_2O_5	**0**	0.03	0.82	< 0.01	0.10
Cr_2O_3	**0**	0.00	0.14	< 0.01	0.02
NiO	**0**	0.01	< 0.01	< 0.01	< 0.01
V_2O_5	**0**	0.00	0.13	< 0.01	< 0.01
ZrO_2	**0**	0.01	< 0.01	< 0.01	< 0.01
SO_3	**0**	0.00	1.63	21.30	1.85
ZnO	**0**	0.00	0.02	< 0.01	< 0.01
Nb_2O_5	**0**	0.00	0.03	< 0.01	< 0.01
SrO	**0**	0.00	< 0.01	0.03	0.02
LOI	**0**	0.10	9.23	10.40	24.10
Total	**100**	**99.92**	**99.90**	**100.00**	**99.99**

Note: LOI is loss of ignition.

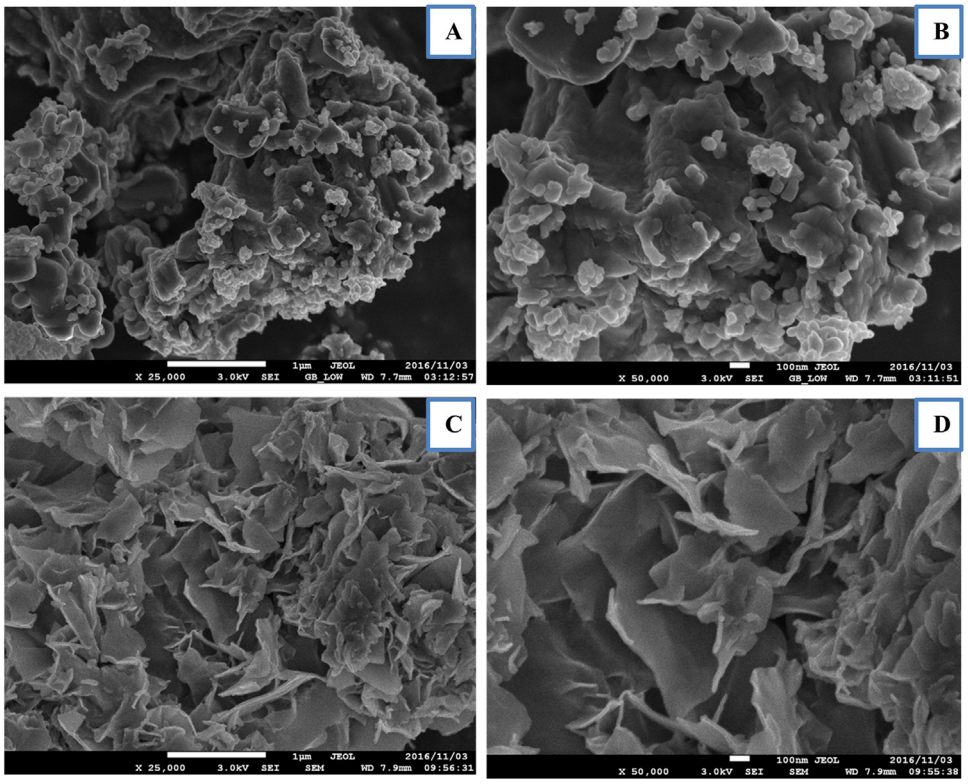

Fig. 4. SEM images of raw magnesite (A and B) and AMD-reacted magnesite (C and D).

calcine cryptocrystalline magnesite with AMD, the content of Fe, Al and Sulphate in the resultant residues were high hence indicating that there was precipitation of chemical species from AMD during the reaction process. This corresponds very well with the quality of product water and the XRD results. Similar results were reported by Masindi, Ndiritu and Maree [69]. Ca and S were also observed to be resent at notable levels hence indicating a possible precipitation of gypsum. This can also be confirmed by XRD results. Mg was also observed to have increased in the product residue hence indicating the formation of brucite as depicted by the XRD peaks. After bubbling CO_2, there was an increase in Ca and CO_2 contents thus proving that limestone was formed. The obtained results are well-aligned to the XRD results.

3.4. Scanning Electron Microscope (SEM) analysis

SEM was utilized to assess the change in morphology of the starting materials and resulting solid residues. Fig. 4**(A) and (B)** shows the morphology of calcined cryptocrystalline magnesite at different magnifications. Fig. 4**(C) and (D)** shows the morphological changes that took place after interaction of calcined cryptocrystalline magnesite with AMD.

As shown in Fig. 4, before contacting AMD, the morphology of calcined cryptocrystalline magnesite contained spherical and leafy like shaped structures hence indicating that the material is heterogeneous. After contacting the AMD, there was platelet; sheet and rod-like structures which were observed hence indicating that there was precipitation of metals from the treatment of acid mine drainage. This verifies the results obtained from XRF and XRD. Bulky solution precipitation could be responsible for the formation of mineral phases which are deposited in-between the secondary residues to form fibre-like, rod shaped and grape structured lumps of tetrahedral folding appearances, thereby acting as a binding link between the micro-particles hence the dense lumps observed in the SEM micrographs. Three main features are observed in the solid residues by SEM technique Fig. 4**(C) and (D)**.

- Appearance of spherical, rod and fibre-like and aggregated lump-like structures indicates formation of new mineral phases in the solid residues.
- Rods-like structures of varying length and thickness/some are flat shaped and are observed over the whole solid residue samples. Lumps with aggregated substances that are lamella and rose-like shaped.
- Aggregation of the small particles forming lumps and rod and grape tetrahedral folding appearances and shaped structures with varying sizes hence confirming the deposition of new mineral phases.
- Sheet of flowers like structures outflowing in a petal fashion and arrangement.

The SEM images of industrial grade lime, synthesized gypsum and industrial grade gypsum are shown in Fig. 5**(A) –(F)**.

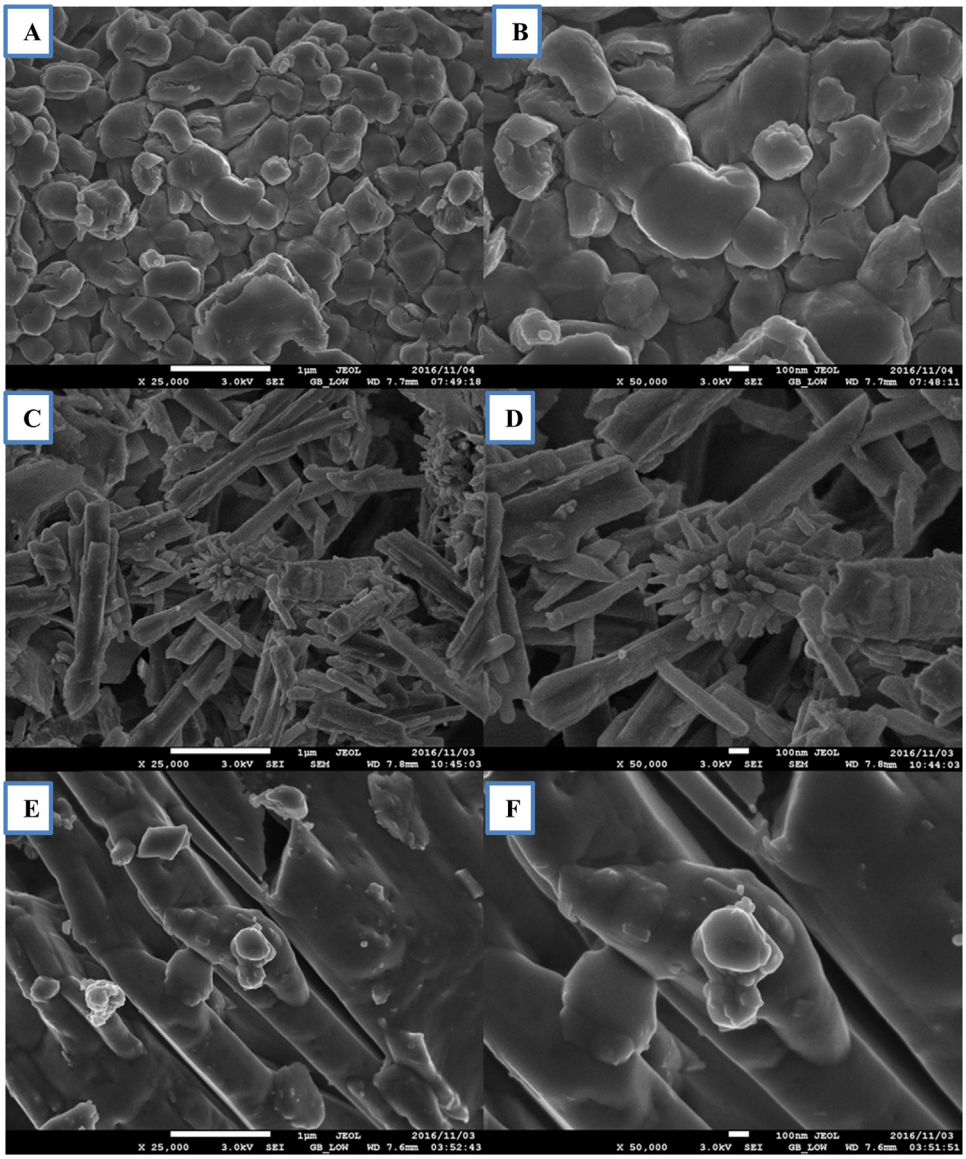

Fig. 5. SEM images of industrial grade lime (A and B), synthesized gypsum (C and D) and industrial grade gypsum (E and F).

The industrial grade lime was observed to have spherical and compacted morphology. The synthesized gypsum showed the presence of rod like structures and aggregated rods. Similar results were observed for industrial grade gypsum. This shows that the synthesized product is gypsum with minor impurities as indicated by the XRD.

The synthesized limestone and industrial grade limestone are shown in Fig. 6**(A)–(D).**

Both synthesized and industrial grade limestone contained some rod and carrots like structures. The morphology was homogenous hence indicating that the recovered material in very pure and contain less impurities.

3.5. High Resolution Transmission Electron Microscopy (HR-TEM) analyses

The TEM diffraction mapping and micrographs of synthesized gypsum are shown in Fig. 7.

The TEM micrographs indicated the presence of rod like structures Fig. 7(E) and (F)). This was conforming to the results reported in SEM micrographs (Fig. 7(C) and (D)). The HR TEM mapping indicated that the rods contains Ca, O and S hence proving that the material that is being synthesized is $CaSO_4$ (Fig. 7(A)–(D)). This was further supported by the XRD results. The precipitation of Sulphur could also be better explained by the product water and XRF results.

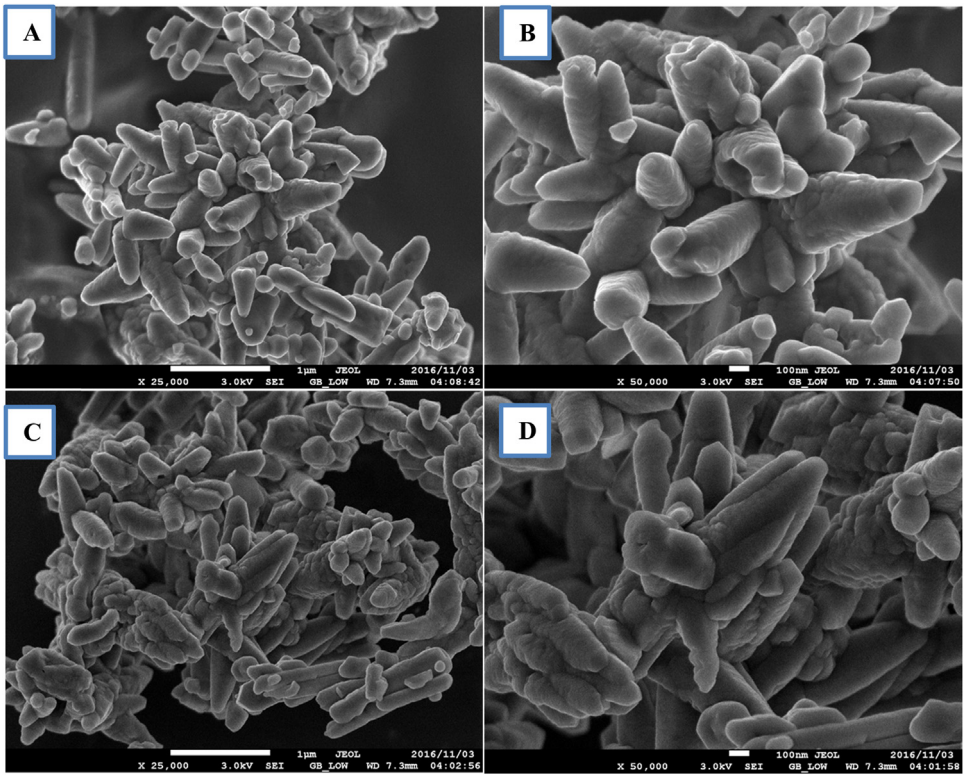

Fig. 6. SEM images of synthesized limestone (A and B) and industrial grade limestone (C and D).

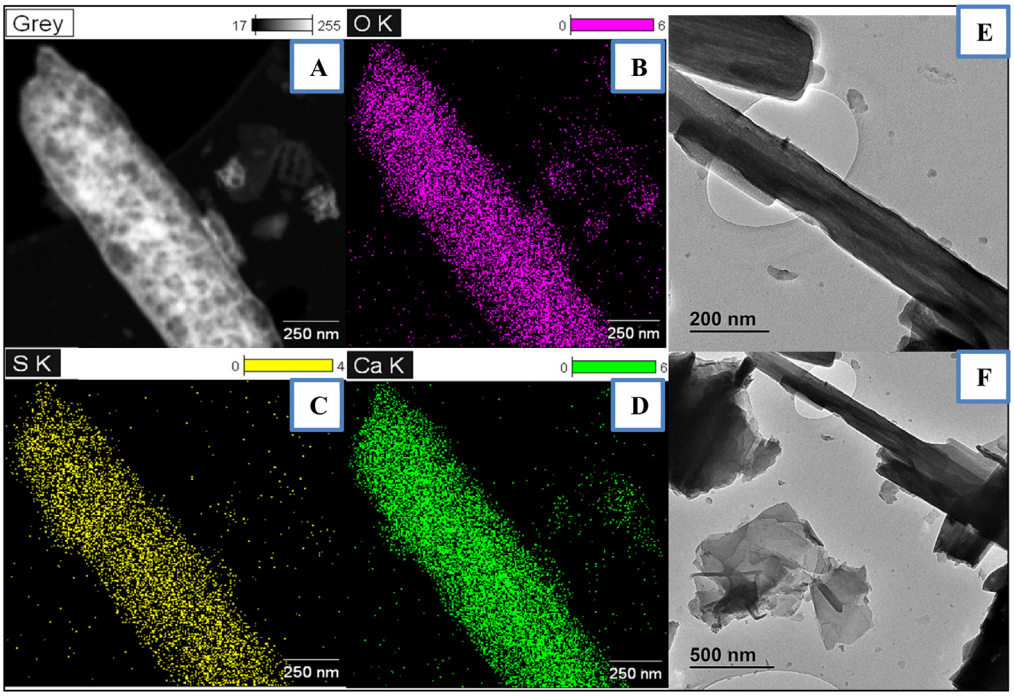

Fig. 7. TEM diffraction mapping and micrographs of synthesized gypsum.

Table 3
Surface area of hydroxide, gypsum and limestone.

Surface area	Magnesite	Gypsum	Limestone
Single point surface area:	15.7822 m^2/g	32.9168 m^2/g	25.1219 m^2/g
BET Surface Area:	15.8087 m^2/g	34.0091 m^2/g	25.8115 m^2/g
Langmuir Surface Area:	21.7524 m^2/g	47.1429 m^2/g	35.9956 m^2/g

3.6. Surface area

The surface area of hydroxide, gypsum and limestone are shown in Table 3.

As shown in Table 3, the obtained results revealed that the surface area of recovered hydroxides was the lowest, followed by limestone and gypsum. This is an indication that these materials can be used as additives to a number of metallurgical processes.

3.7. Thermal stability

Thermogravimetric Analysis (TGA) is a method used to determine the amount of weight loss in a material as a function of increasing temperature, or isothermally as a function of time, in an atmosphere of nitrogen, helium, air, other gas, or in vacuum [70]

Thermal stability of hydroxide, gypsum and limestone are shown in Fig. 8.

TGA plots obtained from the hydroxide, gypsum and limestone analyses are shown in Fig. 8. All chemical components showed some weight loss with an increase in temperature. Hydroxide and gypsum showed the same trends. A sharp decrease in weight (%) at 400 °C is attributed to the loss of hydroxyl groups from the mineral matrices and interlayers. For limestone, two stages of weight loss were observed. There is one at 400 °C which indicates a water loss and another one at 700 °C which indicate the release of CO_2 during the thermal conversion of limestone to lime. Sdiri, Higashi, Hatta, Jamoussi and Tase [71] reported that $CaCO_3$ decompose at 740–990 °C.

3.8. FTIR

The recovered and synthesized Fe-species/minerals were further investigated using FTIR analysis as shown in Fig. 9.

The functional groups for metals hydroxide, gypsum and limestone are shown in Tables 4–6 below. The obtained results corroborate the XRD results which surfaced the presence of gypsum, quartz and calcite for metals hydroxide (Table 4). The functional groups of recovered metals hydroxides are shown in Table 4.

The functional groups of synthesized gypsum are shown in Table 5.

As confirmed by XRD and FTIR results, the synthesized material was rich in sulphate, quartz and hydroxyl group. This is consistent to the XRD and XRF results.

The functional groups of recovered metals hydroxides are shown in Table 6.

As shown in Table 6, the synthesized limestone was observed to be rich in carbonates, quartz and hydroxyl ions. This aligns very well to the XRD and XRF results. It also confirms the major weight loss in TGA results because OH group was escaping with an increase in temperature. Moreover, the carbonate fraction was also escaping due to thermal activation leading to the formation of CaO.

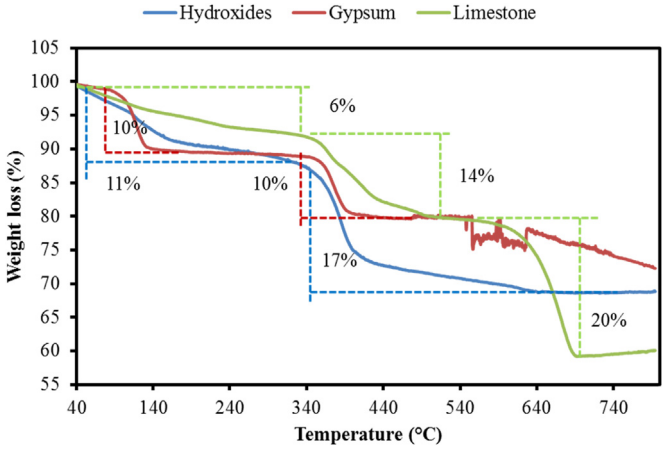

Fig. 8. Thermal stability of hydroxide, gypsum and limestone.

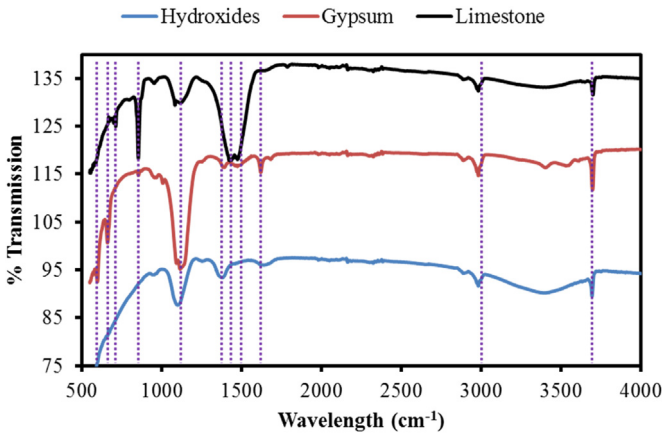

Fig. 9. The recovered and synthesized Fe-species/minerals.

Table 4
Functional groups for metals hydroxide recovered from the treatment of acid mine drainage [69,71].

Vibration	Wavelength range (cm^{-1})
CO_3^{2-} In-plane bending	950
SO_4^{2-} asymmetric stretch	1132
CO_3^{2-} asymmetric stretch	1382
Quartz vibration	900–1200
Hydroxyl ions	2990–4000

Table 5
Functional groups synthesized gypsum [69,72].

Vibration	Wavelength range (cm^{-1})
H–O–H stretching vibration	3310–3650
H–O–H bending vibration	1620
SO_4^{2-} asymmetric stretch	1132
SO_4^{2-} bending vibration	600–666
Quartz vibration	900–1132
Hydroxyl ions	2990–4000

Table 6
Functional groups for metals hydroxide recovered from the treatment of acid mine drainage [69,71].

Vibration	Wavelength range (cm^{-1})
CO_3^{2-} In-plane bending	714
CO_3^{2-} Out-plane bending	860
Duplex CO_3^{2-} asymmetric stretch	1412
Quartz vibration	900–1200
Hydroxyl ions	2990–4000

4. Techno-economic evaluation

This study will only focus on the operational expenditure for the treatment process. Table 7, shows the operational expenditure for the running of the proposed plant.

As shown in Table 7, it can only cost R230.4 (19 USD) to produce a kilolitre (KL) of treated water and R806.40 (66 USD) to produce 3.5 KL of treated water using the proposed technology. However, from the resale of the recovered materials such as Fe-based minerals from the hydroxide reactor, gypsum from the lime reactor and limestone from CO_2 reactor a net profit of R11263.60 (933 USD) may be recovered. This indicates that, the operators can spend R806.40 for treating 3.5 KL of AMD and have a margin profit of R11263.60 (933 USD) from the selling of the recovered products.

Table 7
Operational expenditure of the treatment process and return value.

Operational Expenditure (OPEX)			
	Rand/Litre	Quantity	
AMD	0	3500	0
	Rand/Ton	Required (Kg)	Unit cost per Kg
Magnesite	2500	25	62.5
Lime	2000	280	560
CO_2	1000	100	100
Total			722.5
	Cost/ R	Quantities	Cost per cycle
HCl	50	1	50
Mixer (3 kW)	1.13	10	11.3
Pump (0.75 kW)	1.13	20	22.6
Total			83.9
Grand total			806.4 Per 3.5 KL 230.4 per KL
Recovery	Quantities	Cost/Ton or L	Unit cost
Hydroxides (Kg)	15	1000	15
Gypsum (Kg)	20	2000	40
Limestone (Kg)	10	1500	15
Water (L)	3000	2	R12000.00
Total			R12070.00
Net profit			R11263.60

Note: The costing of this study used South African Rand (R).

5. Conclusion

This study successfully proved that an integration of magnesite, lime, and CO_2 bubbling (MLC process) can be used to treat acid mine drainage (AMD) and produce valuable products such as:

- Water suitable for discharge, industrial applications and irrigation purposes was reclaimed.
- Valuable minerals that has commercial value and they includes, Fe-hydroxides, gypsum and limestone.

Recovered and synthesized materials were of high purity (> 75%). This was further confirmed by X-ray diffraction, XRF and FTIR. From ICP-MS, the water results showed that the initial pH of AMD was 2.5 and it increased to pH ≥ 10 and 12 after contacting magnesite and lime respectively. Post CO2 bubbling the pH was reduced to ≤ 7.29 and approximately ≥ 99% and ≥ 95% of chemical species and sulphate were removed from an aqueous system respectively. Techno-economic evaluation indicated that it can cost R806.40 (66 USD) to treat 3.5 KL of acid mine drainage and have a return of R11263.60 (933 USD) from the resale of the recovered materials. From, the findings of this study, it can be concluded that this novel study will go a long way in curtailing the impact of AMD by recovering and synthesizing valuable materials that have commercial value. The recovery of valuable materials will aid in off-setting the running costs of the treatment process through their resale hence making the technology self-sustaining.

Acknowledgement

The author would wish to express their sincere gratitude to the Council for Scientific and Industrial research (CSIR) for supporting this project. The authors would also like to thank Muedi K. L for proofreading the manuscript.

References

[1] G. Madzivire, W.M. Gitari, V.R.K. Vadapalli, T.V. Ojumu, L.F. Petrik, Fate of sulphate removed during the treatment of circumneutral mine water and acid mine drainage with coal fly ash: modelling and experimental approach, Miner. Eng. 24 (2011) 1467–1477.
[2] V. Masindi, A novel technology for neutralizing acidity and attenuating toxic chemical species from acid mine drainage using cryptocrystalline magnesite tailings, J. Water Process Eng. 10 (2016) 67–77.
[3] D.K. Nordstrom, D.W. Blowes, C.J. Ptacek, Hydrogeochemistry and microbiology of mine drainage: an update, Appl. Geochem. 57 (2015) 3–16.
[4] A. Akcil, S. Koldas, Acid Mine Drainage (AMD): causes, treatment and case studies, J. Clean. Prod. 14 (2006) 1139–1145.
[5] D. Besseling, Taking on the challenges of AMD through horticulture, Water Wheel 12 (2013) 38–39.
[6] S. Jooste, C. Thirion, An ecological risk assessment for a South African acid mine drainage, Water Sci. Technol. 39 (1999) 297–303.
[7] K.K. Kefeni, T.A.M. Msagati, B.B. Mamba, Acid mine drainage: prevention, treatment options, and resource recovery: a review, J. Clean. Prod. 151 (2017) 475–493.
[8] R.T. Amos, D.W. Blowes, B.L. Bailey, D.C. Sego, L. Smith, A.I.M. Ritchie, Waste-rock hydrogeology and geochemistry, Appl. Geochem. 57 (2015) 140–156.
[9] V. Masindi, M.W. Gitari, H. Tutu, M. De Beer, Fate of inorganic contaminants post treatment of acid mine drainage by cryptocrystalline magnesite: complimenting experimental results with a geochemical model, J. Environ. Chem. Eng. 4 (2016) 4846–4856.
[10] V. Bologo, J.P. Maree, F. Carlsson, Application of magnesium hydroxide and barium hydroxide for the removal of metals and sulphate from mine water, Water SA 38 (2012) 23–28.

[11] V. Masindi, M.W. Gitari, H. Tutu, M. DeBeer, Synthesis of cryptocrystalline magnesite–bentonite clay composite and its application for neutralization and attenuation of inorganic contaminants in acidic and metalliferous mine drainage, J. Water Process Eng. 15 (2017) 2–17.
[12] V. Masindi, M.W. Gitari, H. Tutu, M. De Beer, Passive remediation of acid mine drainage using cryptocrystalline magnesite: a batch experimental and geochemical modelling approach, Water SA 41 (2015) 677–682.
[13] K.K. Kefeni, B.B. Mamba, T.A.M. Msagati, Magnetite and cobalt ferrite nanoparticles used as seeds for acid mine drainage treatment, J. Hazard. Mater. 333 (2017) 308–318.
[14] A.S. Sheoran, V. Sheoran, Heavy metal removal mechanism of acid mine drainage in wetlands: a critical review, Miner. Eng. 19 (2006) 105–116.
[15] P.J. Oberholster, P.H. Cheng, A.M. Botha, B. Genthe, The potential of selected macroalgal species for treatment of AMD at different pH rangesin temperate regions, Water Res. 60 (2014) 82–92.
[16] G.S. Simate, S. Ndlovu, Acid mine drainage: challenges and opportunities, J. Environ. Chem. Eng. 2 (2014) 1785–1803.
[17] P. Hobbs, S.H.H. Oelofse, J. Rascher, Management of environmental impacts from coal mining in the upper olifants river catchment as a function of age and scale, Int. J. Water Resour. Dev. 24 (2008) 417–431.
[18] P.J. Hobbs, J.E. Cobbing, Hydrogeological Assessment of Acid Mine Drainage Impacts in the West Rand Basin, Gauteng Province, Hydrogeological Assessment of Acid Mine Drainage Impacts in the West Rand Basin, Gauteng Province, 2007.
[19] Y.-T. Li, T. Becquer, J. Dai, C. Quantin, M.F. Benedetti, Ion activity and distribution of heavy metals in acid mine drainage polluted subtropical soils, Environ. Pollut. 157 (2009) 1249–1257.
[20] C. Lin, Y. Wu, W. Lu, A. Chen, Y. Liu, Water chemistry and ecotoxicity of an acid mine drainage-affected stream in subtropical China during a major flood event, J. Hazard. Mater. 142 (2007) 199–207.
[21] N. López-González, J. Borrego, J.A. Morales, B. Carro, O. Lozano-Soria, Metal fractionation in oxic sediments of an estuary affected by acid mine drainage (southwestern Spain), Estuar. Coast. Shelf Sci. 68 (2006) 297–304.
[22] H.Y. Xiao, W.B. Zhou, F.P. Zeng, D.S. Wu, Water chemistry and heavy metal distribution in an AMD highly contaminated river, Environ. Earth Sci. 59 (2009) 1023–1031.
[23] R. Zick, High density sludge process reduces AMD volume, operating costs at pennsylvania coal mine site, Coal Age 116 (2011) 64–67.
[24] J.P. Maree, P. Du Plessis, Neutralization of acid mine water with calcium carbonate, Water Sci. Technol. 29 (1994) 285–296.
[25] C.E. Zipper, J.G. Skousen, Influent water quality affects performance of passive treatment systems for acid mine drainage, Mine Water Environ. 29 (2010) 135–143.
[26] A. Luptakova, S. Ubaldini, E. Macingova, P. Fornari, V. Giuliano, Application of physical–chemical and biological–chemical methods for heavy metals removal from acid mine drainage, Process Biochem. 47 (2012) 1633–1639.
[27] A. Luptakova, S. Ubaldini, P. Fornari, E. MacIngova, Physical-chemical and biological-chemical methods for treatment of acid mine drainage, Chem. Eng. Trans. (2012) 115–120.
[28] X. Li, H.X. Dai, X.L. Yang, The generation and treatment of acid mine drainage (in:), Adv. Mater. Res. (2013) 1985–1988.
[29] M. Kalin, A. Fyson, W.N. Wheeler, The chemistry of conventional and alternative treatment systems for the neutralization of acid mine drainage, Sci. Total Environ. 366 (2006) 395–408.
[30] E. Torres, M. Auleda, A sequential extraction procedure for sediments affected by acid mine drainage, J. Geochem. Explor. 128 (2013) 35–41.
[31] R.W. Gaikwad, Review and research needs of active treatment of acid mine drainage by ion exchange, Electron. J. Environ. Agric. Food Chem. 9 (2010) 1343–1350.
[32] D.C. Buzzi, L.S. Viegas, M.A.S. Rodrigues, A.M. Bernardes, J.A.S. Tenório, Water recovery from acid mine drainage by electrodialysis, Miner. Eng. 40 (2013) 82–89.
[33] M. Zhang, Adsorption study of Pb(II), Cu(II) and Zn(II) from simulated acid mine drainage using dairy manure compost, Chem. Eng. J. 172 (2011) 361–368.
[34] T. Motsi, N.A. Rowson, M.J.H. Simmons, Adsorption of heavy metals from acid mine drainage by natural zeolite, Int. J. Mineral. Process. 92 (2009) 42–48.
[35] D. Mohan, S. Chander, Removal and recovery of metal ions from acid mine drainage using lignite—a low cost sorbent, J. Hazard. Mater. 137 (2006) 1545–1553.
[36] W.M. Gitari, L.F. Petrik, O. Etchebers, D.L. Key, C. Okujeni, Utilization of fly ash for treatment of coal mines wastewater: solubility controls on major inorganic contaminants, Fuel 87 (2008) 2450–2462.
[37] T. Falayi, F. Ntuli, Removal of heavy metals and neutralisation of acid mine drainage with un-activated attapulgite, J. Ind. Eng. Chem. 20 (2014) 1285–1292.
[38] Y. Chen, K. Gao, H. Lin, Y. Dong, H. Wang, Y. Li, H. Huo, L. Cao, Adsorption properties of microbe resistant to lead and zinc on Zn2+ and Pb2+ in acid mine drainage (AMD), Zhongnan Daxue Xuebao (Ziran Kexue Ban.)/J. Cent. South Univ. (Sci. Technol.) 44 (2013) 1741–1746.
[39] F.I. Ramírez-Paredes, T. Manzano-Muñoz, J.C. Garcia-Prieto, G.G. Zhadan, V.L. Shnyrov, J.F. Kennedy, M.G. Roig, Biosorption of heavy metals from acid mine drainage onto biopolymers (chitin and α (1,3) β-D-glucan) from industrial biowaste exhausted brewer's yeasts (Saccharomyces cerevisiae L.), Biotechnol. Bioprocess Eng. 16 (2011) 1262–1272.
[40] S. Groudev, P. Georgiev, I. Spasova, M. Nicolova, Bioremediation of acid mine drainage in a uranium deposit, Hydrometallurgy 94 (2008) 93–99.
[41] A.P.P. Freitas, I.A.H. Schneider, A. Schwartzbold, Biosorption of heavy metals by algal communities in water streams affected by the acid mine drainage in the coal-mining region of Santa Catarina state, Brazil, Miner. Eng. 24 (2011) 1215–1218.
[42] Y.F. Chen, L.X. Cao, H. Lin, Y.B. Dong, H. Cheng, H.X. Huo, Adsorption of Cu2+ from simulated acid mine drainage by herb-medicine residues and wheat bran, Zhongguo Youse Jinshu Xuebao/Chin. J. Nonferrous Met. 23 (2013) 1775–1782.
[43] A. Çabuk, P. Aytar, S. Gedikli, Y.K. Özel, E. Kocabiyik, Biosorption of acidic textile dyestuffs from aqueous solution by Paecilomyces sp. isolated from acidic mine drainage, Environ. Sci. Pollut. Res. 20 (2013) 4540–4550.
[44] O. Gibert, J. de Pablo, J.L. Cortina, C. Ayora, Treatment of acid mine drainage by sulphate-reducing bacteria using permeable reactive barriers: a review from laboratory to full-scale experiments, Rev. Environ. Sci. Biotechnol. 1 (2002) 327–333.
[45] C.A. Becerra, E.L. López-Luna, S.J. Ergas, K. Nusslein, Microcosm-based study of the attenuation of an acid mine drainage-impacted site through biological sulfate and iron reduction, Geomicrobiol. J. 26 (2009) 9–20.
[46] L. Giloteaux, R. Duran, C. Casiot, O. Bruneel, F. Elbaz-Poulichet, M. Goñi-Urriza, Three-year survey of sulfate-reducing bacteria community structure in Carnoulès acid mine drainage (France), highly contaminated by arsenic, FEMS Microbiol. Ecol. 83 (2013) 724–737.
[47] K.B. Hallberg, New perspectives in acid mine drainage microbiology, Hydrometallurgy 104 (2010) 448–453.
[48] J.N. Zvimba, J. Mulopo, L.T. Bologo, M. Mathye, An evaluation of waste gypsum-based precipitated calcium carbonate for acid mine drainage neutralization, Water Sci. Technol. 65 (2012) 1577–1582.
[49] J.N. Zvimba, M. Mathye, V.R.K. Vadapalli, H. Swanepoel, L. Bologo, Fe(II) oxidation during acid mine drainage neutralization in a pilot-scale sequencing batch reactor, Water Sci. Technol. 68 (2013) 1406–1411.
[50] Y.J. Zheng, Y.L. Peng, C.H. Li, Treatment of acid mine drainage by two-step neutralization, Zhongnan Daxue Xuebao (Ziran Kexue Ban.)/J. Cent. South Univ. (Sci. Technol.) 42 (2011) 1215–1219.
[51] F.M. Romero, L. Núñez, M.E. Gutiérrez, M.A. Armienta, A.E. Ceniceros-Gómez, Evaluation of the potential of indigenous calcareous shale for neutralization and removal of arsenic and heavy metals from acid mine drainage in the Taxco mining area, Mexico, Arch. Environ. Contam. Toxicol. 60 (2011) 191–203.
[52] V.R. Kumar Vadapalli, M.J. Klink, O. Etchebers, L.F. Petrik, W. Gitari, R.A. White, D. Key, E. Iwuoha, Neutralization of acid mine drainage using fly ash, and strength development of the resulting solid residues, S. Afr. J. Sci. 104 (2008) 317–322.
[53] L. Alakangas, E. Andersson, S. Mueller, Neutralization/prevention of acid rock drainage using mixtures of alkaline by-products and sulfidic mine wastes, Environ. Sci. Pollut. Res. 20 (2013) 7907–7916.
[54] H. Zhao, B. Xia, J. Qin, J. Zhang, Hydrogeochemical and mineralogical characteristics related to heavy metal attenuation in a stream polluted by acid mine drainage: a case study in Dabaoshan Mine, China, J. Environ. Sci. 24 (2012) 979–989.
[55] C.M. Zammit, L.A. Mutch, H.R. Watling, E.L.J. Watkin, The recovery of nucleic acid from biomining and acid mine drainage microorganisms, Hydrometallurgy 108 (2011) 87–92.

[56] E. Macingova, A. Luptakova, Recovery of metals from acid mine drainage by selective sequential precipitation processes, in: Proceedings of the 11th International Multidisciplinary Scientific Geoconference and EXPO - Modern Management of Mine Producing, Geology and Environmental Protection, SGEM 2011, 2011, pp. 573–578.
[57] F. Macías, M.A. Caraballo, T.S. Rötting, R. Pérez-López, J.M. Nieto, C. Ayora, From highly polluted Zn-rich acid mine drainage to non-metallic waters: implementation of a multi-step alkaline passive treatment system to remediate metal pollution, Sci. Total Environ. 433 (2012) 323–330.
[58] G. Lee, J.M. Bigham, G. Faure, Removal of trace metals by coprecipitation with Fe, Al and Mn from natural waters contaminated with acid mine drainage in the Ducktown Mining District, Tennessee, Appl. Geochem. 17 (2002) 569–581.
[59] R.A. Kleiv, M. Thornhill, Predicting the neutralisation of acid mine drainage in anoxic olivine drains, Miner. Eng. 21 (2008) 279–287.
[60] V. Sheoran, A.S. Sheoran, R.P. Choudhary, Biogeochemistry of acid mine drainage formation: a review, Mine Drainage and Related Problems, (2011), pp. 119–154.
[61] P.K. Sahoo, K. Kim, S.M. Equeenuddin, M.A. Powell, Current approaches for mitigating acid mine drainage, Rev. Environ. Contam. Toxicol. 226 (2013) 1–32.
[62] S. Pozo-Antonio, I. Puente-Luna, S. Lagüela-López, M. Veiga-Ríos, Techniques to correct and prevent acid mine drainage: a review, DYNA 81 (2014) 73–80.
[63] S. Papirio, D.K. Villa-Gomez, G. Esposito, F. Pirozzi, P.N.L. Lens, Acid mine drainage treatment in fluidized-bed bioreactors by sulfate-reducing bacteria: a critical review, Crit. Rev. Environ. Sci. Technol. 43 (2013) 2545–2580.
[64] D.B. Johnson, K.B. Hallberg, Acid mine drainage remediation options: a review, Sci. Total Environ. 338 (2005) 3–14.
[65] G. Madzivire, R.M. Maleka, M. Tekere, L.F. Petrik, Cradle to cradle solution to problematic waste materials from mine and coal power station: acid mine drainage, coal fly ash and carbon dioxide, J. Water Process Eng. (2017).
[66] V. Masindi, Recovery of drinking water and valuable minerals from acid mine drainage using an integration of magnesite, lime, soda ash, CO_2 and reverse osmosis treatment processes, J. Environ. Chem. Eng. 5 (2017) 3136–3142.
[67] C.T. Benatti, C.R.G. Tavares, E. Lenzi, Sulfate removal from waste chemicals by precipitation, J. Environ. Manag. 90 (2009) 504–511.
[68] V. Masindi, M.W. Gitari, H. Tutu, M. De Beer, Fate of inorganic contaminants post treatment of acid mine drainage by cryptocrystalline magnesite: complimenting experimental results with a geochemical model, J. Environ. Chem. Eng. 4 (2016) 4846–4856.
[69] V. Masindi, J.G. Ndiritu, J.P. Maree, Fractional and step-wise recovery of chemical species from acid mine drainage using calcined cryptocrystalline magnesite nano-sheets: an experimental and geochemical modelling approach, J. Environ. Chem. Eng. (2018).
[70] A. Al-Majed, A.H.H. Bakheit, H.A. Abdel Aziz, H. Alharbi, F.I. Al-Jenoobi, Chapter Five - Pioglitazone, in: H.G. Brittain (Ed.), Profiles of Drug Substances, Excipients and Related Methodology, Academic Press, 2016, pp. 379–438.
[71] A. Sdiri, T. Higashi, T. Hatta, F. Jamoussi, N. Tase, Mineralogical and spectroscopic characterization, and potential environmental use of limestone from the Abiod formation, Tunisia, Environ. Earth Sci. 61 (2010) 1275–1287.
[72] S.-G. Jeong, S.J. Chang, S. Wi, J. Lee, S. Kim, Energy performance evaluation of heat-storage gypsum board with hybrid SSPCM composite, J. Ind. Eng. Chem. 51 (2017) 237–243.